

Performance Comparison of Several Published Tissue Near-Infrared Spectroscopy Algorithms

S. J. Matcher, C. E. Elwell, C. E. Cooper,* M. Cope, and D. T. Delpy

University College London Department of Medical Physics and Bioengineering, 1st Floor Shropshire House, 11-20 Capper Street, London WC1E 6JA, United Kingdom; and *University College London Department of Paediatrics, The Rayne Institute, University Street, London WC1E 6JJ, United Kingdom

Received August 23, 1994

We have collected multiwavelength near-infrared (NIR) attenuation spectra on human forearm muscle, the adult rat head, and newborn piglet head to compare the changes in chromophore concentration derived from these data using published algorithms from four groups. We find differences between the results from the algorithms on each data set, particularly in their estimation of cytochrome oxidase (cyt-*aa*₃) redox changes. We also find some differences when applying the same algorithm to the three data sets, suggesting possible difficulties in transferring algorithms between different physiological systems (e.g., Kurth, C. D., Steven, J. M., Benaron, D., and Chance, B. (1993) *J. Clin. Monit.* 9, 163–170). We have also compared the algorithms using simulated data generated using measured hemoglobin absorption spectra and a diffusion model for light transport in tissue. We find that while the algorithms from three groups are in broad agreement, that published by Piantadosi (Piantadosi, C. A. (1993) *Methods Toxicol.* 2, 107–126) produces significantly different results for cyt-*aa*₃ and HbO₂. Either the hemoglobin spectra used to produce the simulated data are inaccurate or the modeling is incorrect, or this algorithm is erroneous. © 1995 Academic Press, Inc.

Tissue near-infrared spectroscopy measures concentration changes of various substances in living tissue by detecting changes in the near-infrared tissue attenuation spectrum (1). The technique now finds wide application to research problems particularly in the study of cerebral hemodynamics (2–7) and oxygen transport to muscle (8–10). The mathematical formula which converts the measured changes in light attenuation at various wavelengths into corresponding concentration changes for the substances of interest (especially deoxyhemoglobin (Hb), oxyhemoglobin (HbO₂), and cyto-

chrome *aa*₃ redox state (cyt-*aa*₃)¹) is generally termed an “algorithm.” Research groups and NIR instrument manufacturers around the world currently employ a variety of different measurement wavelengths and algorithms, which raises the possibility that certain *in vivo* observations may be artifacts of a particular algorithm rather than genuine physiological phenomena. This may be particularly true of apparent changes in the redox state of the cyt-*aa*₃ enzyme, the NIR signal that reflects directly on the normality of cell respiration (39). The low *in vivo* concentration of this enzyme leads to difficulties in separating its signal from the generally much larger signals due to Hb and HbO₂ (11).

This paper describes the use of a continuous wavelength charge-coupled device (CCD)-based tissue spectrometer to collect *in vivo* data which can then be processed using almost any published algorithm, thus allowing the direct comparison of these algorithms. By applying the algorithms to synthetic data generated using what we believe are accurate *in vitro* hemoglobin spectra, we can also identify those algorithms which, in the modeled geometry, produce cross-talk between their derived cytochrome-*aa*₃ and hemoglobin values. Such algorithms are either erroneous or are constructed using hemoglobin spectra very different from our data. To help make this distinction, we include our measured Hb/HbO₂ absorption spectra (12) measured from 650 nm to beyond 1 μm in tabular form in the Appendix.

DESCRIPTION OF THE *IN VIVO* MEASUREMENTS

We have used our CCD-based tissue spectrometer (13) to collect near-infrared attenuation spectra from approximately 650 to 1000 nm with a dispersion of 1.1 nm per CCD pixel and a resolution of approximately 4 nm during one clinical and two animal studies. One of the

¹Abbreviations used: cyt-*aa*₃, cytochrome *aa*₃; NIR, near infrared; CCD, charge-coupled device; DPF, differential pathlength factor.

algorithms being compared was specifically developed for use on the adult rat head and so we have included a data set of spectra collected on an adult rat head during cerebral hypoxia induced by 100% nitrogen inhalation. In order to determine how well such algorithms can be transferred to other physiological systems, we have also tested the algorithms on data sets collected on the human forearm muscle during cuff ischemia and on the head of a newborn piglet subject to a hypoxic-ischemic insult. The detailed measurement protocols were as follows.

(1) *Cerebral hypoxia in an adult rat.* Source and detector probes were placed against the skull of an anesthetized (urethane, 0.5 ml/100 g body wt), ventilated adult rat (after removal of scalp tissues and temporal muscles) in a transillumination configuration. The top of the skull was painted black (using a cellulose-based automobile paint) and a light-tight tape was attached to prevent light leakage from the source to the detector. The resulting source/detector separation was approximately 14 mm. A brief (25 s) period of cerebral hypoxia was induced by increasing inspired N_2 to 100%.

(2) *Forearm ischemia in an adult volunteer.* Source and detector optical fibers were placed 35 mm apart traversing the forearm muscle of a healthy 28-year-old male adult volunteer (midway between the elbow and the wrist). The fibers were located in an arm support and the forearm was then laid onto the support, so that a reflection geometry was achieved. A 3-mm-thick pad of black plastic between the source and detector fiber locations was used to block any stray light propagating directly from the source to the detector. A black cloth was wrapped around the arm and fibers to eliminate stray room light. The forearm was supported horizontally and roughly at heart level with the palm of the hand facing down; the separation between the fibers was perpendicular to the long axis of the forearm. By choosing this orientation of the fibers we deliberately attempted to illuminate several muscle groups. A blood pressure cuff placed around the upper arm was rapidly inflated to 240 mm Hg to occlude arterial and venous blood flow. The cuff was maintained at this pressure for 5 min and then rapidly deflated. Spectra were collected at 5-s intervals throughout the occlusion and recovery period.

(3) *Cerebral hypoxia-ischemia in a newborn piglet.* As part of a project to investigate the mechanisms of neonatal hypoxic-ischemic brain damage (14), a newborn piglet was subjected to such an insult by occlusion of the carotid arteries combined with mild hypoxia (inspired oxygen reduced to 12% for 50 min). This insult has been shown to lead to significant drops in energy metabolites (especially phosphocreatine and ATP as measured by ^{31}P NMR spectroscopy) in the rabbit brain (15), and similar changes are observed in this piglet model (16). Source and detector fibers for the NIR measurements were fixed 4 cm apart across the top of the

skull and held in contact with the skin using a stereotactic holder. The skull was sufficiently domed to preclude the possibility of light propagating directly from the source to the detector. Blackout material was deemed unnecessary as the piglet was placed several feet inside the bore of an NMR magnet and the lights inside the magnet enclosure were switched off. Spectra were collected at 30-s intervals during the 150-min study.

The resulting data sets consist of a time series of intensity spectra. These are converted to a time series of attenuation changes by dividing each spectrum into the spectrum measured at time zero and taking the base 10 logarithm. In order to obtain concentration changes in millimolar units, the attenuation change is also divided by the product of the source/detector fiber separation (in centimeters) and the estimated differential pathlength factor (DPF) (17,18) for the particular physiological model. For the purposes of this comparison, whole figure DPF values of 4 for the human forearm and 5 for the rat and piglet heads (wavelength independent) have been used. The rat and forearm DPF estimates are derived from *in vivo* time-of-flight measurements obtained in transmission (rat head) and reflection (human forearm). The DPF value for the newborn piglet head is assumed to approximately equal that of the human neonate measured *in vitro* and in reflection. It should be noted that since the DPF value used is independent of wavelength, its precise numeric value affects the results simply by scaling the derived Hb, HbO_2 , and cyt-aa_3 chromophore traces equally; it does not affect the direction of any changes or the amplitudes of the chromophore traces relative to each other. Hence, arguments concerning trends (e.g., whether total hemoglobin volume rises or falls or whether cyt-aa_3 goes oxidized or reduced) are unaffected by the DPF value used.

DESCRIPTION OF THE FOUR COMPARED ALGORITHMS

Although many papers have been published describing measurements made with NIRS, to our knowledge only four groups have published details of the algorithms used in the analysis of the data and these are compared here.

UCL

This is a generalized algorithm determining concentration changes for Hb, HbO_2 , and cyt-aa_3 . The concentrations are derived using multilinear regression given the specific absorption coefficients for Hb, HbO_2 , and cyt-aa_3 (oxidized minus reduced) measured on purified solutions of the compounds (12). To compensate for tissue-scattering effects, the coefficients for each wavelength are scaled by the measured DPF at that wavelength (19). Data have been published allowing coefficients for any specific wavelength to be employed. A laser-diode-based NIR spectrometer has been developed

by UCL (20) and one version of this (the NIRO500, Hamamatsu Photonics KK, Japan) uses four wavelengths, yielding an algorithm termed UCL4 which in matrix notation has the form

$$\begin{pmatrix} \Delta\text{Hb} \\ \Delta\text{HbO}_2 \\ \Delta\text{Cyt} \end{pmatrix} = \begin{pmatrix} 1.58 & -1.35 & -0.57 & 0.68 \\ -0.66 & -0.85 & 0.56 & 1.5 \\ -0.26 & 1.17 & 0.12 & -0.92 \end{pmatrix} \times \begin{pmatrix} \Delta\text{OD}_{775\text{nm}} \\ \Delta\text{OD}_{810\text{nm}} \\ \Delta\text{OD}_{870\text{nm}} \\ \Delta\text{OD}_{904\text{nm}} \end{pmatrix}, \quad [1]$$

where ΔOD represents the change in detected optical density at the wavelength given in the subscript.

There is also a six-wavelength instrument (NIRO-1000, Hamamatsu Photonics KK, Japan) employing a six-coefficient version of the algorithm (UCL6):

$$\begin{pmatrix} \Delta\text{Hb} \\ \Delta\text{HbO}_2 \\ \Delta\text{Cyt} \end{pmatrix} = \begin{pmatrix} 1.56 & -0.51 & -0.78 & -0.57 & -0.023 & 0.65 \\ -0.55 & -0.72 & -0.39 & 0.12 & 0.74 & 1.31 \\ -0.3 & 0.65 & 0.6 & 0.26 & -0.26 & -0.83 \end{pmatrix} \times \begin{pmatrix} \Delta\text{OD}_{775\text{nm}} \\ \Delta\text{OD}_{800\text{nm}} \\ \Delta\text{OD}_{825\text{nm}} \\ \Delta\text{OD}_{850\text{nm}} \\ \Delta\text{OD}_{875\text{nm}} \\ \Delta\text{OD}_{900\text{nm}} \end{pmatrix}. \quad [2]$$

Alternatively, when using data obtained with the CCD spectrometer, one can use all available wavelengths over some range, typically (and throughout this paper) 770–900 nm, i.e., 112 wavelengths. We denote this algorithm UCL n .

This algorithm makes no assumptions about tissue scattering or geometry (other than that the wavelength dependence of pathlength in the tissue of interest approximates those of the adult human head, arm, and leg averaged). It ignores, however, multiple scattering effects such as the nonlinear relationship between absorption and attenuation (11) and might thus exhibit poor performance when detecting the weak signals of cyt- aa_3 .

SAPPORO

This is a three-wavelength algorithm for determining Hb, HbO₂, and cyt- aa_3 changes by solving simultaneous

equations (21). Changes in baseline attenuation (due to scattering changes and/or source/detector efficiency fluctuations) are compensated by measuring attenuation differences between the measuring wavelengths and a fourth reference wavelength. The algorithm was developed specifically for observations on the intact rat head, in which the plane of illumination is vertical, through the roof of the mouth to the top of the skull (surface tissues not removed). The coefficients used in this algorithm were derived from measurements on suspensions of whole blood, either fully oxy- or fully deoxy-, by measuring the change of light attenuation caused by the suspension as a function of hematocrit. The algorithm assumes that a spectral region exists in which the cyt- aa_3 difference spectrum displays zero absorption, the reference wavelength then being selected to lie in this region. The authors of the algorithm suggest that 750 nm fulfills this criterion (21). (We would suggest that the authors' statement in Fig. 4 of Ref. (21), that 805 nm can be used as a reference wavelength, appears to be inconsistent with this requirement given the published form of their CuA difference spectrum (22)).

$$\begin{pmatrix} \Delta\text{Hb} \\ \Delta\text{HbO}_2 \\ c_3 \cdot \Delta\text{Cyt} \end{pmatrix} = \begin{pmatrix} 0.749 & -1.587 & 0.0 \\ -0.898 & -2.1 & 0.0 \\ 1.53 & -0.763 & 1.0 \end{pmatrix} \times \begin{pmatrix} \Delta\text{OD}_{700\text{nm}} - \Delta\text{OD}_{750\text{nm}} \\ \Delta\text{OD}_{730\text{nm}} - \Delta\text{OD}_{750\text{nm}} \\ \Delta\text{OD}_{805\text{nm}} - \Delta\text{OD}_{750\text{nm}} \end{pmatrix}. \quad [3]$$

Unlike the other algorithms compared in this study, this algorithm does not attempt to quantify the cyt- aa_3 signal relative to the Hb and HbO₂ signals; hence, the constant c_3 is arbitrary (but positive given the measurement and reference wavelengths assumed here (21,22)).

The hemoglobin coefficients are derived using measurements made on whole (i.e., scattering) samples of blood placed in a 1-cm pathlength cuvette. Since red blood cell scattering represents only a small fraction of total tissue scattering, spectral distortions induced *in vivo* should dominate those induced in these reference hemoglobin spectra and one might expect the resulting algorithm to be as transferrable as the generic UCL algorithm. Since the algorithm is calibrated exclusively for observations of the rat head, corrections for the longer pathlengths found in other systems must be made explicitly by the user. It should be noted that the assumption concerning the form of the cyt- aa_3 difference spectrum is contentious (38).

DUKE-P

This is a four-wavelength algorithm for determining Hb, HbO₂, and cyt- aa_3 changes and changes in a fourth unidentified compound by solving simultaneous

equations (23). The coefficients have been determined *in vivo* by measuring reflectance spectra from the intact cat brain. The fourth signal is generally discarded, yielding the following three equations for Hb, HbO₂, and cyt-*aa*₃:

$$\begin{pmatrix} \Delta\text{Hb} \\ \Delta\text{HbO}_2 \\ \Delta\text{Cyt} \end{pmatrix} = \begin{pmatrix} 2.20 & -0.91 & 0.19 & -0.86 \\ -1.51 & 0.57 & -0.24 & 1.48 \\ -3.08 & 6.52 & -0.66 & -2.45 \end{pmatrix} \times \begin{pmatrix} \Delta\text{OD}_{775\text{nm}} \\ \Delta\text{OD}_{810\text{nm}} \\ \Delta\text{OD}_{870\text{nm}} \\ \Delta\text{OD}_{904\text{nm}} \end{pmatrix}. \quad [4]$$

This algorithm is the only one of the four to use chromophore spectra measured *in vivo* (in the cat head). The difference between spectra obtained in extreme hyperoxia with blood present and then with blood completely exchanged with perfluorocarbon is taken as an estimate of the *in vivo* HbO₂ spectrum. The difference spectrum obtained by then inducing anoxia (in the presence of perfluorocarbon) is taken to represent the *in vivo* cyt-*aa*₃ difference spectrum. Finally, the difference spectrum obtained by exchanging the perfluorocarbon with fully deoxygenated blood in the anoxic brain is taken to represent the *in vivo* Hb spectrum.

The measured spectra should thus include realistic contributions from tissue scattering, in particular realistic wavelength-dependent pathlengths. *A priori* one might thus expect this algorithm to transfer accurately to similar large structures such as the piglet head and the human forearm, but less well to small transilluminated structures such as the rat head.

Since the measurement of the HbO₂ spectrum is performed by inducing extreme hyperoxia, there is a risk that the spectrum may be contaminated by small amounts of Hb since the concentration of Hb will never fall completely to zero. Also the spectra obtained in the anoxic state may be distorted by scattering to a different degree than those obtained in hyperoxia since there is evidence for scattering changes in anoxia due to cell death (17). The appearance of a second peak in the cyt-*aa*₃ difference spectrum is also contentious (22,38).

KEELE

This is a three-wavelength algorithm for determining Hb, HbO₂, and cyt-*aa*₃ changes by solving simultaneous equations. The Hb coefficients used in this algorithm were determined by measurements on whole blood and the cytochrome data from *in vitro* measurements on the purified enzyme (24,25). Recently the Keele group have scaled these coefficients using the UCL DPF data (26).

$$\begin{pmatrix} \Delta\text{Hb} \\ \Delta\text{HbO}_2 \\ \Delta\text{Cyt} \end{pmatrix} = \begin{pmatrix} 1.642 & -1.02 & -0.221 \\ -1.157 & 0.081 & 1.776 \\ -0.014 & 0.635 & -0.611 \end{pmatrix}$$

$$\times \begin{pmatrix} \Delta\text{OD}_{775\text{nm}} \\ \Delta\text{OD}_{845\text{nm}} \\ \Delta\text{OD}_{904\text{nm}} \end{pmatrix} \quad [5]$$

This algorithm differs from the generic UCL algorithms only in the number of wavelengths used and in that the hemoglobin spectra (but *not* the cytochrome spectrum) are measured in whole blood, i.e., in a scattering solution, which will alter the shape of the spectra due to path-lengthening effects. However, as with the SAPPORO algorithm, we expect that since scattering due to red blood cells represents only a small fraction of total tissue scattering, both this and the UCL algorithm should suffer similar errors when applied *in vivo*.

USE OF PUBLISHED ALGORITHMS FROM OTHER GROUPS WITH OUR CCD DATA

Since the aim of this paper is to apply published algorithms from various groups to a selection of common data sets, it is clearly important to ensure that the algorithms are applied consistently. Each algorithm described above has been developed for use on a particular near-infrared system. However, as discussed above and as described in the quoted references, each algorithm is designed to convert *changes in measured light attenuation* into corresponding changes in tissue chromophore concentration. The fundamental measurement parameter is thus a ratio of detected light fluxes at two distinct times and as such should be essentially independent of any specific instrument factors with the exception of spectral bandwidth and resolution. Thus, the coefficients of each algorithm should depend only on (a) the extinction coefficients of the chromophores of interest at the measurement wavelengths, (b) the wavelength-dependent pathlength factors (DPFs), which are a consequence of the diffusive nature of light propagation through tissue and which are *dependent only on the tissue optical properties and source/detector spacing (and to a lesser extent the measurement geometry)*, and (c) the spectral bandwidth over which the change in light attenuation has been measured. The only plausible exception to this might be a system where the source/detector fiber diameters were large compared to their separation, in which case a significant (and both fiber diameter and wavelength dependent) range of optical pathlengths would be sampled. The diameters of the fiber bundles used in the studies presented here are 5 mm; hence, this condition should not occur in the forearm or piglet studies but will apply in the rat study.

The UCL/KEELE/DUKE-P algorithms are intended for use with NIR tissue spectrometers using pulsed laser diode light sources which generally have output spectral bandwidths of 3–4 nm. This is virtually identical to the spectral resolution of our CCD spectrometer so that the coefficients of these algorithms should be immediately

applicable to our CCD data. The SAPPORO algorithm was developed for use with a spectrometer using a quartz-halogen light source (identical to that used in our CCD system) and a system of rotating colored filters. To our knowledge the bandwidth of these filters has not been published and hence all results presented here effectively assume a filter bandwidth of 4 nm. Cope (12) has analyzed the effects of filter bandwidth on the measurement accuracy of light attenuation changes in the NIR, concluding that for a simple tissue spectrum in which light attenuation is simply a linear function of wavelength, attenuation differences of 0.1 OD across the filter bandpass result in measurement errors of order 1%. The effects of finite bandwidth can be easily incorporated into the CCD data simply by smoothing the raw intensity spectra so that the spectrometer can effectively simulate any other tissue near-infrared spectrometer.

RESULTS

Figures 1, 2, and 3 show the results of applying these six algorithms to the three experimentally measured data sets.

For the rat brain transient hypoxia study, the animal is mechanically ventilated and the hypoxia is N₂ induced. We would expect only a little vasodilation until late in the insult when blood pressure begins to change and hence little change in cerebral blood volume. The early parts of the Hb and HbO₂ changes should therefore be equal and opposite with Hb rising and then falling. Since cyt-aa₃ has a low K_m for oxygen, its redox state need not change in concordance with hemoglobin (11,21,27,28) (although this point is disputed by some authors (29,30)). We thus expect a delayed reduction of cyt-aa₃ during the course of the hypoxia with a rapid recovery when the oxygen supply is restored. Such behavior is shown clearly by the three UCL algorithms and by the KEELE algorithm. The DUKE-P algorithm shows the expected behavior for Hb and HbO₂ but with an immediate and large cyt-aa₃ response of peak magnitude 65 μM . The SAPPORO algorithm detects a reduction of cyt-aa₃ together with a substantial rise in total hemoglobin (i.e., the Hb concentration rise substantially exceeds the HbO₂ concentration fall). The time delay between the HbO₂ and cyt-aa₃ traces is small (1–2 s) compared to that in the UCL and KEELE traces (~ 20 s).

For the forearm ischemia study, if the occlusion pressure is rapidly applied, then there should be little change in total blood volume (although blood pooling due to gravity may produce some small volume change). During the occlusion desaturation should occur, producing an increase in Hb and a virtually equal decrease in HbO₂. Cytochrome-aa₃ would be expected to show only a small, delayed reduction due its low K_m for O₂, the large oxygen reserve bound to muscle myoglobin, and the low oxygen consumption in resting muscle (31). The SAPPORO algorithm is unique in showing an apparently substantial fall in blood volume

during ischemia. The DUKE-P algorithm produces a large and immediate cyt-aa₃ reduction of approximately 60 μM . The UCL and KEELE algorithms show only small cyt-aa₃ changes and generally in the direction of increased oxidation (NB different cyt-aa₃ scales are used for the different figures). If our physiological expectations are correct, then we must conclude that these algorithms are producing questionable results for cyt-aa₃. The UCL algorithms, particularly UCL_n, show evidence of cross-talk between cyt-aa₃ and hemoglobin during the reactive hyperemia phase. The SAPPORO algorithm detects a slight cyt-aa₃ oxidation during the first half of the occlusion and a slight reduction during the second half.

For the piglet cerebral hypoxia-ischemia data, the occlusion of flow is only partial and so the Hb and HbO₂ swings need not be equal and opposite. Here one would expect a reduction of cyt-aa₃ of greater magnitude than that observed for muscle ischemia given the lack of a myoglobin oxygen reserve and higher oxygen consumption. In this study all algorithms with the exception of SAPPORO show similar time courses for Hb and HbO₂, although the absolute magnitudes vary between 30 and 40 μM . Again the SAPPORO algorithm is unique in apparently detecting a substantial blood volume rise. All six algorithms also show clear reductions of cyt-aa₃. The UCL and KEELE algorithms show a gradual reduction, the absolute magnitudes (peak) being 9 and 2.5 μM , respectively. The SAPPORO and DUKE-P algorithms show immediate cyt-aa₃ reduction, the magnitude being approximately 60 μM for the latter algorithm.

COMPARISON OF THE ALGORITHMS ON SIMULATED DATA

In addition to comparing these algorithms on experimental *in vivo* data, where there is uncertainty over the true chromophore concentration changes, we have also compared them on a synthetic data set.

This artificial data set consists of a time series of absolute attenuation spectra which have been generated using an analytical diffusion theory relation between light attenuation and the absorption and scattering coefficients of a medium (32). Diffusion theory has been shown to be an accurate model of light transport in tissue for tissue thicknesses in excess of a few millimeters (33) and is now widely used in the field of tissue optics. The relation used here applies to an infinite slab and has the form

$$A = -\log_{10} \left(\frac{\sinh(\sigma/\mu'_s)}{\sinh(\sigma\rho)} \cdot \frac{1}{\sqrt{2\pi}} \right) \quad (6)$$

$$(\sigma = \sqrt{3 \cdot \mu_a \cdot (\mu_a + \mu'_s)}),$$

where ρ is the source/detector separation, μ_a is the absorption coefficient, and μ'_s is the transport scattering coefficient of the medium.

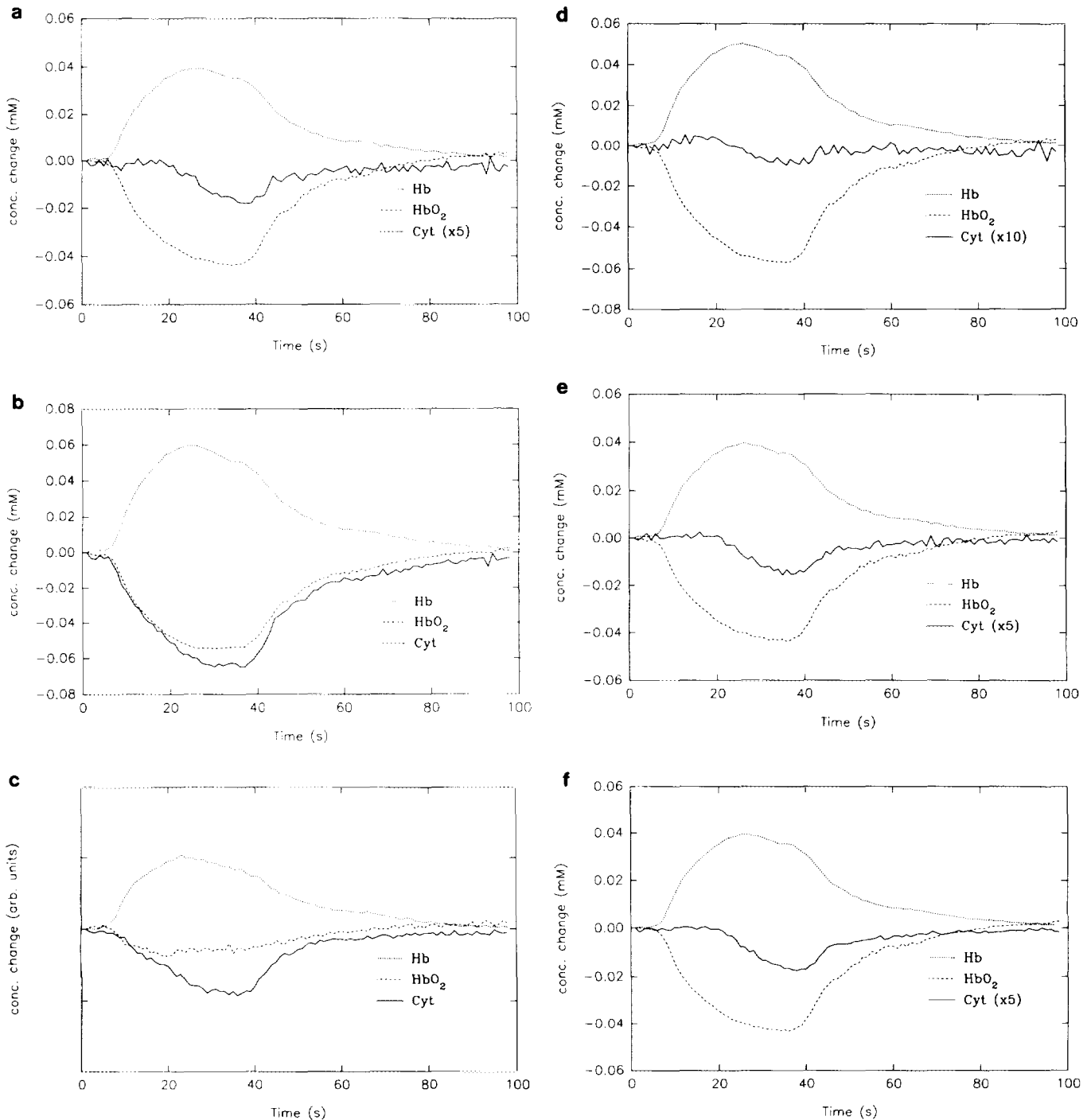


FIG. 1. The six algorithms applied to the adult rat cerebral hypoxia data. After removal of surface tissues, the intact skull of an anesthetized ventilated adult rat has been transilluminated by NIR light and changes in attenuation spectrum monitored at 1-s intervals during a transient period of hypoxia. Each algorithm has been used to derive concentration changes for Hb, HbO₂, and cyt-aa₃ using identical values for optode spacing (14 mm) and DPF (5.0). (a) UCL4, (b) DUKE-P, (c) SAPPORO, (d) KEELE, (e) UCL6, and (f) UCLn.

To generate the time series we have taken measured *in vitro* spectra of the two dominant oxygen-dependent compounds, Hb and HbO₂ (12), and combined them in concentrations which vary with time over clinically realistic ranges. Figure 4 shows the measured Hb and

HbO₂ spectra used. In the time series, each of the chromophores varies independently of the other in a total of 10 combinations, to allow one to assess the magnitude of any cross-talk effects in the algorithms. Figure 5 shows the resulting time-dependent traces for the two chromo-

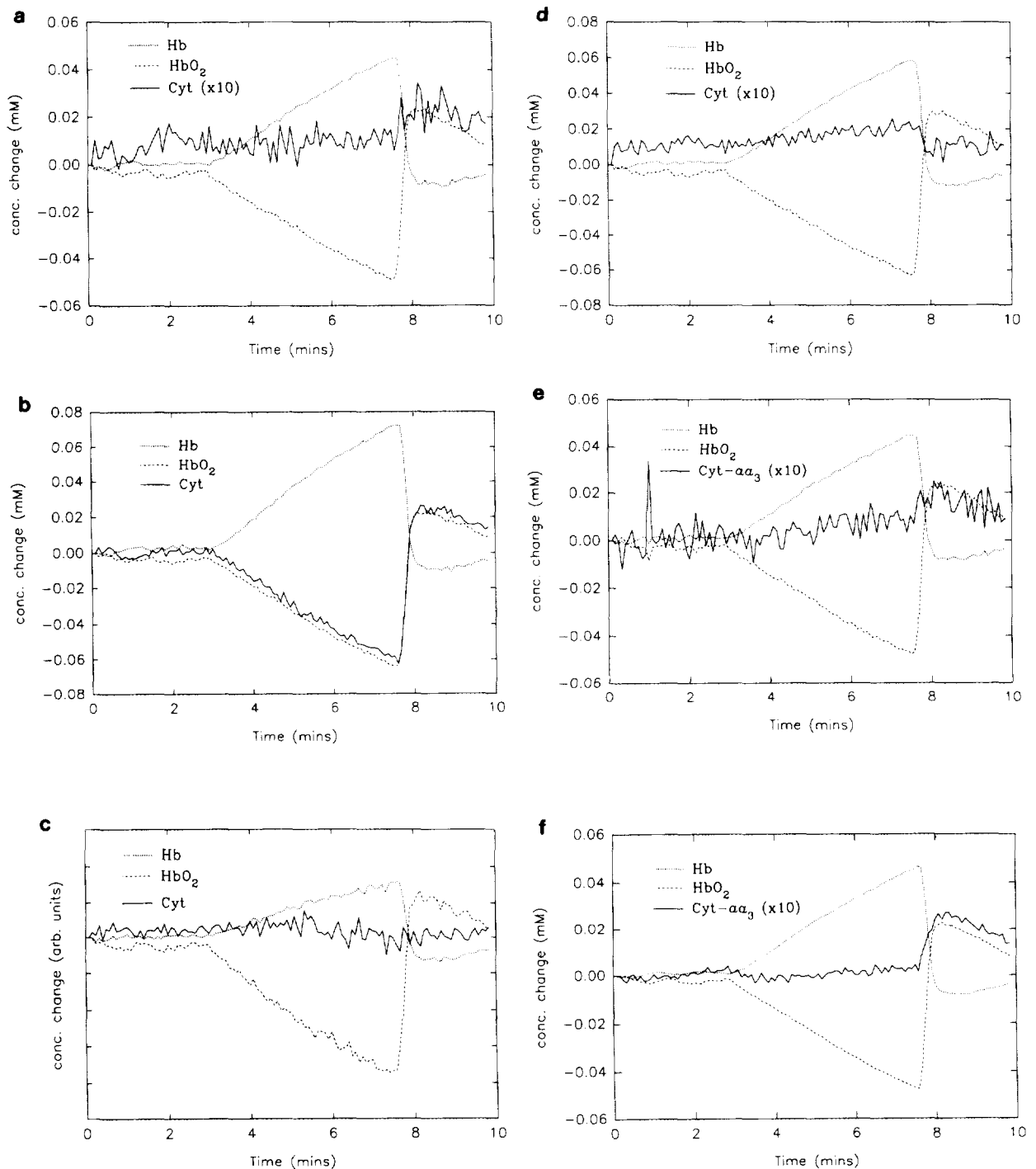


FIG. 2. The six algorithms applied to the adult forearm ischemia data. A rapidly inflated cuff has been used to produce a desaturation in the forearm muscle of an adult volunteer and the resulting changes in the tissue NIR attenuation spectrum have been monitored at 5-s intervals. The optode spacing was approximately 35 mm and a DPF value of 4.0 was assumed. (a) UCL4, (b) DUKE-P, (c) SAPPORO, (d) KEELE, (e) UCL6, and (f) UCLn.

phores. Hb varies between 0 and 40 μM and HbO₂ varies between 20 and 60 μM . The two chromophore spectra are then linearly combined in these time-dependent concentrations (together with a fixed contribution from tissue water at 80% concentration) to yield the overall $\mu_a(\lambda, t)$.

Using the Hb, HbO₂, and H₂O absorptions alone, the overall tissue absorption coefficient is lower than that suggested by *in vitro* measurements. van der Zee and colleagues (34,35) have obtained absorption and scattering coefficient spectra on *in vitro* samples of rat brain tissue

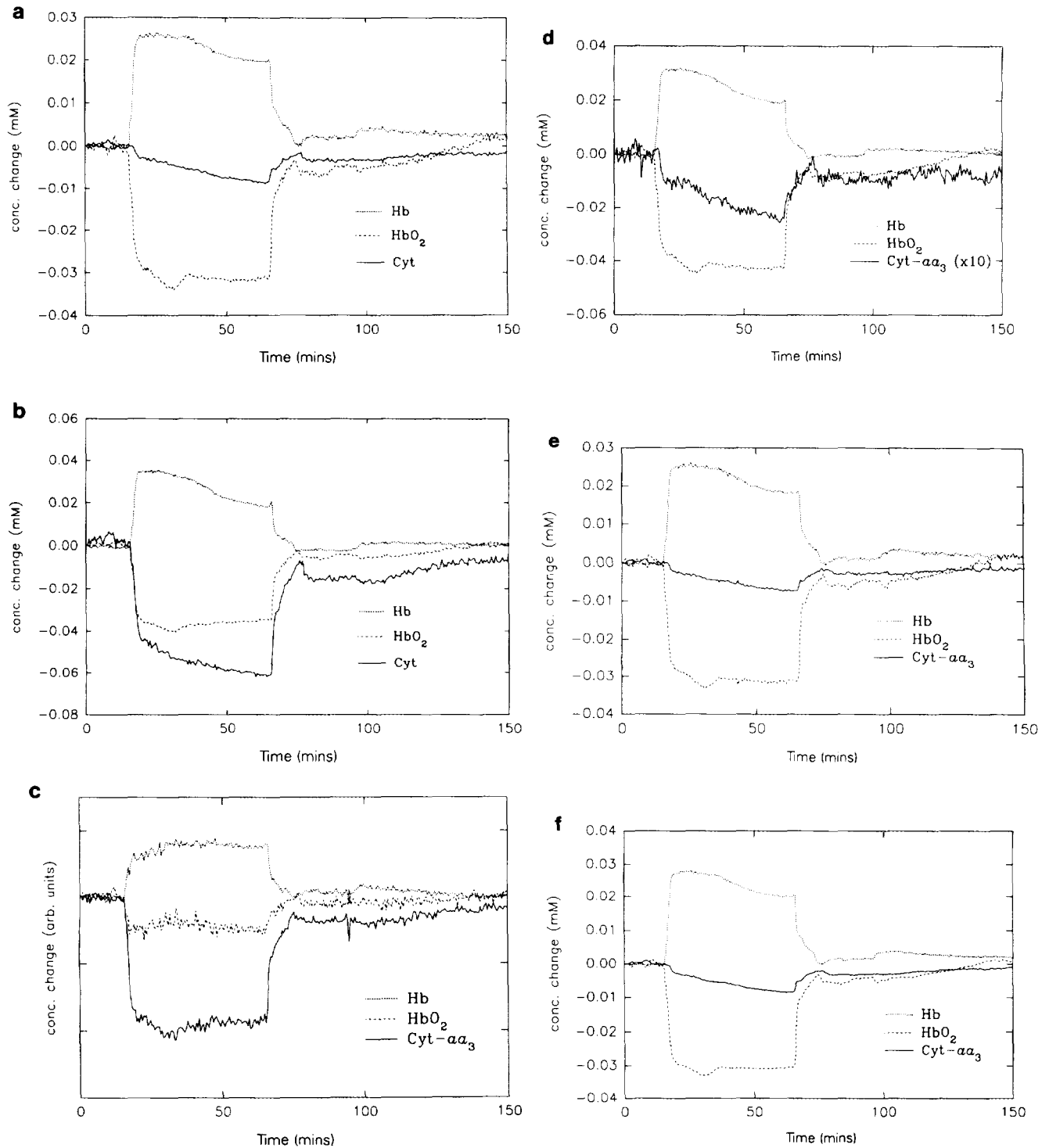


FIG. 3. The six algorithms applied to the piglet cerebral hypoxic-ischemia data. The analysis of Figs. 1 and 2 has been repeated on a data set obtained on the intact head of a piglet during a hypoxic-ischemic insult of the type described in Ref. (16). The values of optode spacing and DPF used were 40 mm and 5.0, respectively. (a) UCL4, (b) DUKE-P, (c) SAPPORO, (d) KEELE, (e) UCL6, and (f) UCL n .

using measurements of diffuse reflectance and transmittance which yield an estimate for μ_a at 820 nm of approximately 0.14 OD cm^{-1} . The corresponding value obtained using the reference spectrum for Hb at $60 \mu\text{M}$

concentration is only approximately 0.05 OD cm^{-1} , which suggests that tissue also contains significant quantities of other absorbers. To take some account of this, we have modified the simulated absorption coeffi-

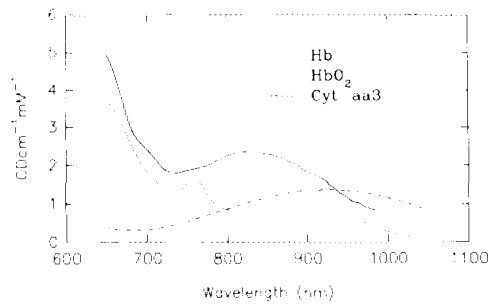


FIG. 4. The measured *in vitro* specific absorption coefficient spectra for Hb and HbO₂ used to generate the synthetic data sets. We also show our measured, *in vitro*, oxidized minus reduced cyt-aa₃ difference spectrum (which is dominated by the light absorption spectrum of the enzyme metal center copper A (Cu_A)). The hemoglobin absorption spectra were measured at University College London on lysed blood samples.

cient spectrum by adding a fixed baseline μ_b of 0.07 OD cm^{-1} (wavelength and time independent) in order to bring the absorption coefficient at 820 nm into closer agreement with the data of van der Zee *et al.* This extra μ_b term is thus assumed to account for all other (oxygen independent) near-infrared-absorbing chromophores in tissue. The resulting absorption coefficient spectra $\mu_a(\lambda, t)$ are then converted to attenuation spectra $A(\lambda, t)$ using Eq. [6] with a source/detector separation of 40 mm. The spectral characteristics of the transport-scattering coefficient spectrum $\mu'_s(\lambda)$ used in this calculation are data measured on *in vitro* rat brain samples (35). Figure 6 illustrates this scattering coefficient spectrum, while Fig. 7 gives an example of the resulting data set and compares it to real *in vivo* data, with the upper curves showing $A(\lambda, t)$ for a section of the time series representing an hypoxic episode (Hb and HbO₂ rise and fall by equal amounts) and the lower curves showing the corresponding $A(\lambda, t)$ measured on a rat brain during transient hypoxia.

RESULTS USING THE SIMULATED DATA

We have deliberately excluded cytochrome-aa₃ from the synthetic data set so that, *on the assumption that our hemoglobin spectra are correct*, a correct algorithm should produce little measurable cytochrome-aa₃ change, whereas a faulty algorithm will produce a spurious cytochrome-aa₃ trace, highly correlated with the hemoglobin changes. Figure 8 shows the results of applying the six algorithms to the synthetic data set. Figure 8a compares, for each of the six algorithms, the *relative* Hb trace derived by the algorithm with the *absolute* Hb trace used to generate the data. Hence, the two traces are offset. Figures 8b, 8c, and 8d show the corresponding results for HbO₂, cyt-aa₃, and Hbtot (Hb + HbO₂).

All algorithms produce some spurious cyt-aa₃ changes, due to the nonlinearities induced in the measured attenuation spectra by Eq. [6]. However, the DUKE-P algo-

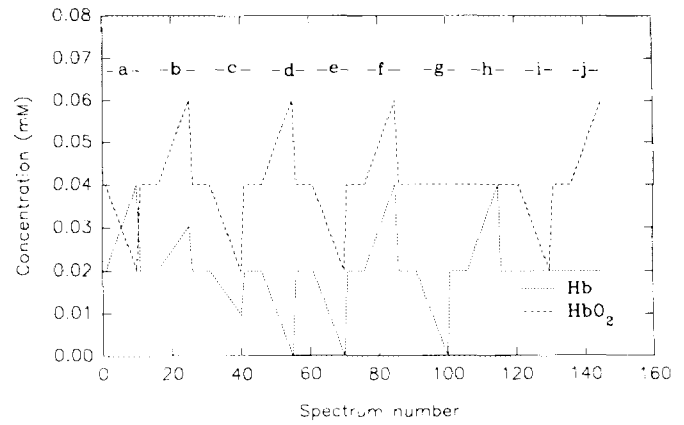


FIG. 5. The time courses of Hb and HbO₂ concentration used to generate the synthetic data set. Hb and HbO₂ vary independently between approximately 10 and 60 μM and mimic a range of clinical phenomena such as hypoxia, hyperoxia, and blood volume changes due to hypercapnia or blood pressure changes: (a) A desaturation with no blood volume change; (b) a blood volume increase at constant (66%) saturation; (c) a blood volume decrease at constant (66%) saturation; (d) an increase in saturation at constant blood volume (hyperoxia); (e) equal drop in Hb and HbO₂, i.e., volume drop at constant HbDiff; (f) equal rise in Hb and HbO₂, i.e., volume rise at constant HbDiff; (g) fall in Hb, constant HbO₂; (h) rise in Hb, constant HbO₂; (i) fall in HbO₂, constant Hb; (j) rise in HbO₂, constant Hb.

rithm produces by far the largest, with cyt-aa₃ tracking HbO₂ closely during ischemic episodes, just as with the *in vivo* data. The algorithm also seems to miscalculate the changes in HbO₂ during episodes representing large blood volume increases, generally underreading the true increase in HbO₂. These episodes also exhibit anomalous cyt-aa₃ changes, with the trace often appearing to mirror the change in Hb.

The SAPPORO algorithm produces Hb and HbO₂ traces which differ from those of UCL and KEELE in apparently overestimating the magnitude of ΔHb relative to ΔHbO_2 . Thus, the algorithm detects an apparent blood volume rise during a simulated desaturation, as shown in Fig. 8d. Interestingly this is the same pattern as with the rat head and piglet head hypoxias.

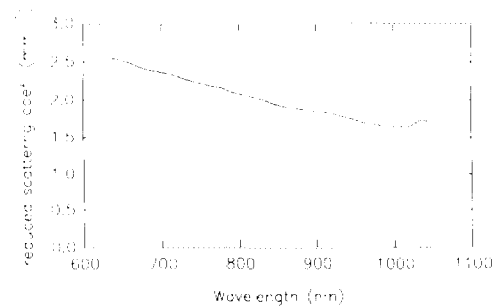


FIG. 6. The tissue-scattering coefficient spectrum used to generate the synthetic data. This spectrum was measured on postmortem samples of adult rat brain using an integrating sphere technique.

The UCL and KEELE algorithms produce very similar results except that the apparent magnitudes of the hemoglobin traces differ by approximately 30%. This indicates that substantial differences exist between the hemoglobin spectra used to generate the two algorithms. The KEELE algorithm uses Hb and HbO₂ spectra measured on whole, intact blood, whereas the UCL algorithms use spectral measurements made on lysed blood samples. Thus, the KEELE spectra will contain features due to scattering from the red blood cells which will be absent in the UCL spectra.

Scale errors exist between the Hb/HbO₂ changes derived by all algorithms and those actually occurring in the synthetic data set. This is to be expected because the quantification of the derived changes is, as previously mentioned, dependent on an assumed value of DPF.

We can summarize the performance of the algorithms in generating spurious cyt-aa₃ signals by quoting the rms value for each cytochrome-aa₃ trace over the time course (excluding the SAPPORO algorithm, which claims only to detect cytochrome trends):

UCL4	0.32 μM
UCL6	0.28 μM
UCLn	0.06 μM
KEELE	0.69 μM
DUKE-P	14.3 μM

The amplitude of the spurious cyt-aa₃ trace generated by the UCL algorithms falls as the number of wavelengths increases. This suggests that the use of an over-determined measurement set may be useful in counteracting the distortions introduced by tissue scattering.

CONCLUSIONS

The estimated *in vivo* concentration of cyt-aa₃ is 3.5 μM in human muscle (36) and 4 μM in newborn piglet brain (C. E. Cooper and G. C. Brown, unpublished data). Thus, the cyt-aa₃ redox changes derived using the KEELE method are reasonable but the changes calculated by UCL4 for the piglet data and DUKE-P for both piglet and human forearm data are too large. For the case of forearm ischemia the change derived by DUKE-P is an order of magnitude larger than the *in vivo* concentration of the enzyme quoted by van Kuilenburg *et al.* and the algorithm seems generally to derive cyt-aa₃ changes which mirror Hb. When used on simulated data generated using Hb and HbO₂ spectra measured at UCL (reproduced in the appendix), the algorithm still produces cyt-aa₃ traces approximately mirroring Hb and also produces spurious HbO₂ traces, particularly during episodes where total hemoglobin concentration changes.

The SAPPORO algorithm, which was originally developed for observations of the rat head using transillumination in a vertical plane, produces plausible results for the cyt-aa₃ redox trend in all three studies but detects substantial changes in blood volume during these same studies, which for the forearm ischemia study in particular seems physiologically unlikely. This algorithm calculates cyt-aa₃ changes by first calculating Hb and HbO₂ changes, subtracting these from the measured total attenuation change and interpreting the residual as the cyt-aa₃ redox change. Hence, the derivation of physiologically unlikely hemoglobin changes must also cast doubt on the validity of the cyt-aa₃ signal. The discrepancies observed in this study may indicate that there are problems when trying to apply an algorithm developed for one system (the rat head with vertical plane transillumination) to others (human muscle in reflection, rat head with transverse illumination, etc.) with different geometries and presumably different scattering properties. In this context it should be noted that algorithms developed for use on large tissue samples (e.g., human muscle or piglet head) can largely ignore the complicating effects of tissue boundaries and treat the probed tissue as a semi-infinite half-space. Theoretical and experimental studies on light transport in scattering media have shown that at optode spacings of more than a few

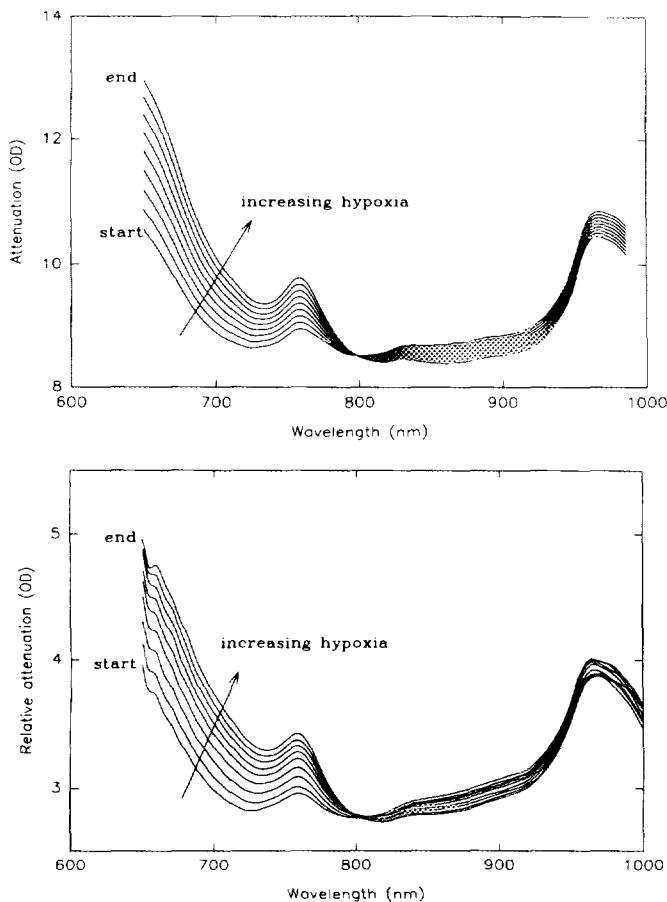


FIG. 7. A comparison of a sample of synthetic attenuation spectra modeling a hypoxic swing (upper graph) with actual *in vivo* attenuation spectra obtained on the adult rat head during a transient hypoxia episode (lower graph).

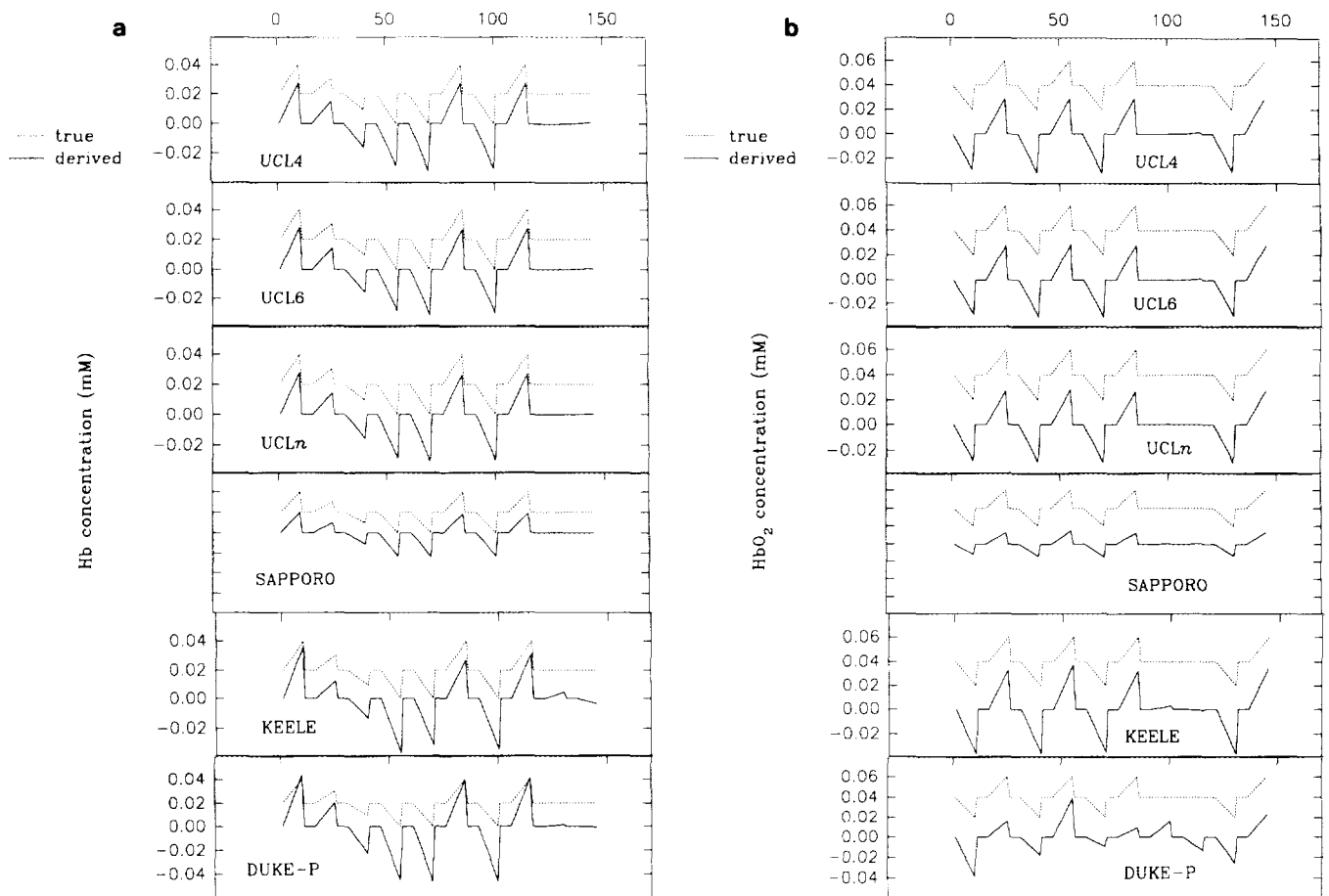


FIG. 8. Concentration changes obtained by applying the six algorithms to the synthetic data set. The four graphs show the results for Hb, HbO₂, cyt-*aa*₃, and Hb_{tot} (Hb + HbO₂) with each plot comparing the *relative* chromophore trace derived by the particular algorithm with the actual *absolute* (and hence offset) chromophore trace used in the simulation. Note the scale in the cyt-*aa*₃ plot for the DUKE-P algorithm, which is 10 times coarser than the scales used for the other algorithms. Note also that we have refrained from quantifying the results of the SAPPORO algorithm because quantified results for hemoglobin changes are only claimed by the inventors when applying the algorithm to a rat head at fixed (~ 1 cm) optode spacing.

centimeters, the DPF in tissue is not very sensitive to geometry (varying from infinite half-space to infinite slab or sphere) (32). It is likely that an algorithm specifically developed on a small geometry such as the rat head may be less transferrable to other larger measuring geometries. Madsen *et al.* (37) have noted that time-resolved estimates of the optical properties of tissue simulating phantoms become increasingly inaccurate as the physical size of the phantom falls. The authors explain this as a consequence of the increasing violation of the assumed boundary conditions (which are those of a semi-infinite half-space) by the phantom.

The simulated data set shows that small spurious cyt-*aa*₃ changes are generated by the UCL and KEELE algorithms, due to the nonlinear relationship between attenuation and absorption coefficient exhibited by media which scatter radiation multiply. Spurious cyt-*aa*₃ results generated by the SAPPORO algorithm could be explained by differences between the hemoglobin spectra

used in this and the UCL and KEELE algorithms, although the lack of quantification of cyt-*aa*₃ in the SAPPORO algorithm precludes detailed discussion of this. On the basis of the synthetic data results, questions are raised as to the accuracy of the DUKE-P algorithm, as published. For this algorithm to be considered a valid detector of cyt-*aa*₃ redox changes, substantial errors must exist in the hemoglobin spectra used in both the UCL (Fig. 4) and KEELE algorithms.

In conclusion, this study clearly illustrates that substantial differences can arise when applying different published algorithms to the same *in vivo* data set. Algorithms which seem to perform adequately in one system can apparently generate unrealistic results when transferred to another system, so that it may be necessary to develop and validate a range of NIR algorithms for use on different tissues and specific geometries. The absolute magnitude and time course of the cyt-*aa*₃ redox changes seem particularly variable between algorithms.

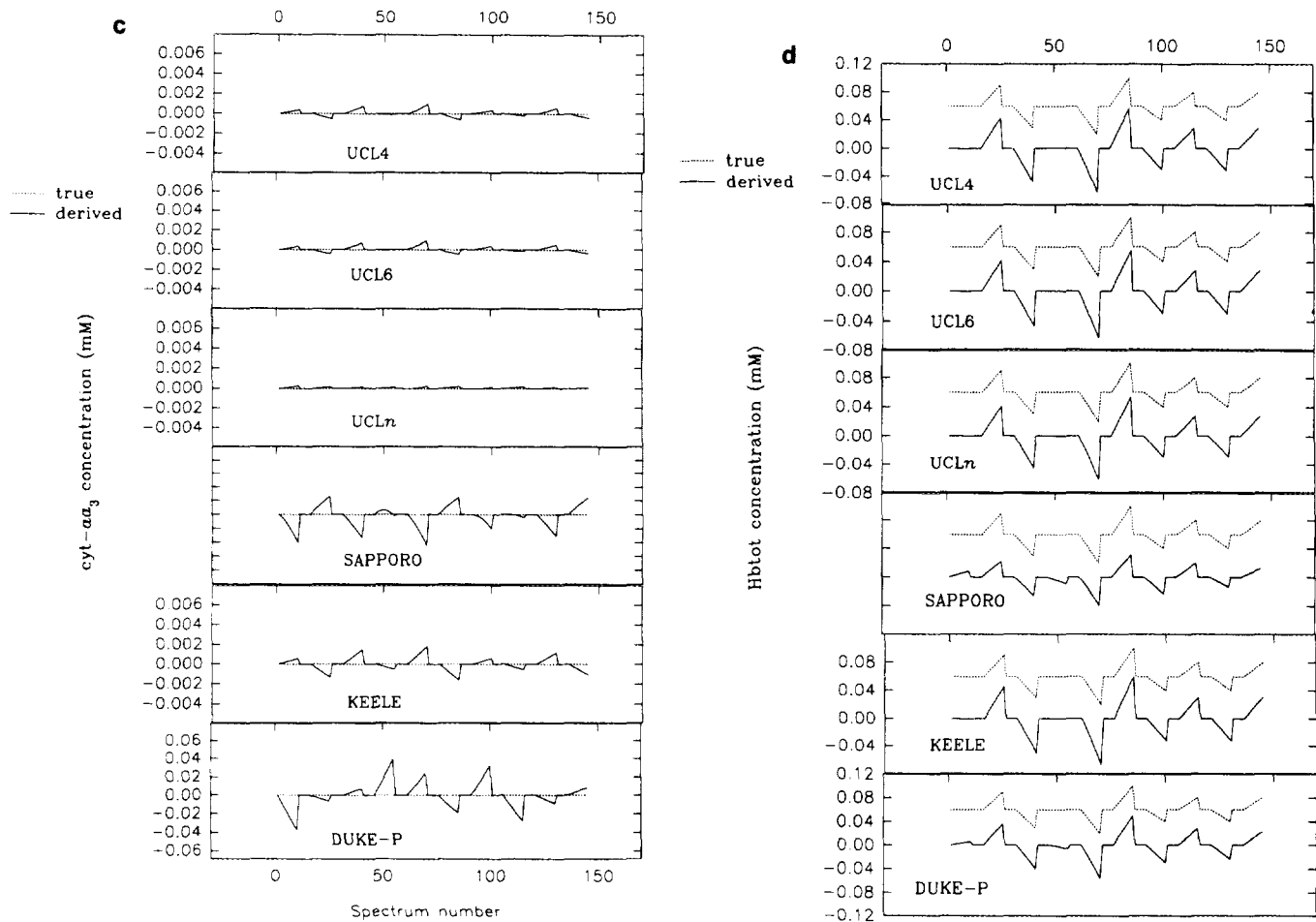


FIG. 8—Continued

This is unfortunate as accurate measurement of the redox state of cyt-aa₃ should give the most direct information concerning the adequacy of oxygen delivery to the cells themselves (39) and as such an increase in cyt-aa₃ reduction is a clearer indicator of the onset of irreversible hypoxic-ischemic brain damage than a drop in blood oxygen content.

The identification of an incorrect algorithm using

data obtained *in vivo* is clearly difficult since the precise physiological responses of various living systems to hypoxia and ischemia are themselves contentious. However, the degree of variability between the algorithms themselves clearly shows that more work in this area is required, particularly if data are to be compared between different groups of workers and if NIRS is to be relied upon as an accurate monitor of tissue oxygenation.

APPENDIX 1

Specific Absorption Coefficients for Hb and HbO₂ (OD cm⁻¹ mm⁻¹) from 650 to 1042 nm
Sampled at 1-nm Intervals

Hb

650	3.7351	716	1.4907	782	1.0571	848	0.7850	914	0.8942	980	0.4233
651	3.7039	717	1.4721	783	1.0372	849	0.7856	915	0.8931	981	0.4146
652	3.6727	718	1.4535	784	1.0173	850	0.7861	916	0.8920	982	0.4061
653	3.6414	719	1.4365	785	0.9975	851	0.7871	917	0.8904	983	0.3975
654	3.6126	720	1.4197	786	0.9822	852	0.7880	918	0.8885	984	0.3892
655	3.5841	721	1.4029	787	0.9668	853	0.7890	919	0.8866	985	0.3810
656	3.5555	722	1.3875	788	0.9515	854	0.7901	920	0.8844	986	0.3729
657	3.5269	723	1.3733	789	0.9385	855	0.7912	921	0.8817	987	0.3648
658	3.4982	724	1.3592	790	0.9264	856	0.7923	922	0.8790	988	0.3567
659	3.4695	725	1.3456	791	0.9143	857	0.7935	923	0.8760	989	0.3487
660	3.4408	726	1.3352	792	0.9034	858	0.7949	924	0.8726	990	0.3409
661	3.4062	727	1.3249	793	0.8939	859	0.7963	925	0.8691	991	0.3334
662	3.3717	728	1.3146	794	0.8844	860	0.7977	926	0.8655	992	0.3259
663	3.3371	729	1.3081	795	0.8752	861	0.7993	927	0.8613	993	0.3187
664	3.2990	730	1.3029	796	0.8676	862	0.8009	928	0.8571	994	0.3117
665	3.2582	731	1.2976	797	0.8600	863	0.8025	929	0.8528	995	0.3047
666	3.2174	732	1.2946	798	0.8524	864	0.8044	930	0.8480	996	0.2978
667	3.1762	733	1.2950	799	0.8461	865	0.8063	931	0.8432	997	0.2909
668	3.1327	734	1.2953	800	0.8399	866	0.8082	932	0.8382	998	0.2841
669	3.0891	735	1.2959	801	0.8338	867	0.8102	933	0.8324	999	0.2776
670	3.0455	736	1.3028	802	0.8285	868	0.8122	934	0.8265	1000	0.2714
671	2.9993	737	1.3096	803	0.8237	869	0.8143	935	0.8207	1001	0.2652
672	2.9519	738	1.3164	804	0.8190	870	0.8166	936	0.8143	1002	0.2592
673	2.9045	739	1.3277	805	0.8146	871	0.8189	937	0.8080	1003	0.2533
674	2.8569	740	1.3411	806	0.8111	872	0.8213	938	0.8016	1004	0.2475
675	2.8087	741	1.3545	807	0.8075	873	0.8237	939	0.7945	1005	0.2419
676	2.7606	742	1.3697	808	0.8040	874	0.8261	940	0.7874	1006	0.2364
677	2.7124	743	1.3887	809	0.8014	875	0.8285	941	0.7802	1007	0.2309
678	2.6652	744	1.4078	810	0.7987	876	0.8310	942	0.7727	1008	0.2257
679	2.6183	745	1.4268	811	0.7961	877	0.8336	943	0.7651	1009	0.2207
680	2.5713	746	1.4501	812	0.7941	878	0.8361	944	0.7575	1010	0.2156
681	2.5248	747	1.4736	813	0.7922	879	0.8387	945	0.7493	1011	0.2109
682	2.4788	748	1.4971	814	0.7904	880	0.8412	946	0.7410	1012	0.2062
683	2.4329	749	1.5212	815	0.7888	881	0.8438	947	0.7327	1013	0.2015
684	2.3870	750	1.5458	816	0.7874	882	0.8463	948	0.7241	1014	0.1971
685	2.3436	751	1.5703	817	0.7861	883	0.8489	949	0.7154	1015	0.1928
686	2.3004	752	1.5938	818	0.7849	884	0.8516	950	0.7068	1016	0.1884
687	2.2572	753	1.6142	819	0.7842	885	0.8542	951	0.6982	1017	0.1844
688	2.2162	754	1.6346	820	0.7834	886	0.8568	952	0.6896	1018	0.1804
689	2.1772	755	1.6549	821	0.7827	887	0.8594	953	0.6810	1019	0.1763
690	2.1382	756	1.6646	822	0.7822	888	0.8620	954	0.6715	1020	0.1726
691	2.0997	757	1.6733	823	0.7817	889	0.8645	955	0.6616	1021	0.1688
692	2.0656	758	1.6820	824	0.7812	890	0.8670	956	0.6517	1022	0.1651
693	2.0315	759	1.6816	825	0.7809	891	0.8694	957	0.6420	1023	0.1618
694	1.9974	760	1.6745	826	0.7808	892	0.8718	958	0.6324	1024	0.1585
695	1.9665	761	1.6674	827	0.7806	893	0.8742	959	0.6229	1025	0.1553
696	1.9370	762	1.6566	828	0.7805	894	0.8765	960	0.6133	1026	0.1522
697	1.9076	763	1.6343	829	0.7804	895	0.8787	961	0.6037	1027	0.1492
698	1.8791	764	1.6121	830	0.7804	896	0.8807	962	0.5941	1028	0.1461
699	1.8530	765	1.5898	831	0.7804	897	0.8827	963	0.5843	1029	0.1432
700	1.8270	766	1.5582	832	0.7804	898	0.8846	964	0.5745	1030	0.1402
701	1.8010	767	1.5259	833	0.7804	899	0.8863	965	0.5647	1031	0.1374
702	1.7777	768	1.4935	834	0.7805	900	0.8880	966	0.5550	1032	0.1347
703	1.7548	769	1.4590	835	0.7805	901	0.8897	967	0.5453	1033	0.1320
704	1.7319	770	1.4229	836	0.7806	902	0.8910	968	0.5357	1034	0.1295
705	1.7099	771	1.3869	837	0.7807	903	0.8923	969	0.5261	1035	0.1272
706	1.6887	772	1.3513	838	0.7809	904	0.8936	970	0.5166	1036	0.1250
707	1.6675	773	1.3169	839	0.7812	905	0.8944	971	0.5071	1037	0.1227
708	1.6464	774	1.2825	840	0.7815	906	0.8952	972	0.4976	1038	0.1205
709	1.6267	775	1.2481	841	0.7817	907	0.8959	973	0.4880	1039	0.1183
710	1.6070	776	1.2175	842	0.7820	908	0.8962	974	0.4785	1040	0.1161
711	1.5873	777	1.1870	843	0.7823	909	0.8965	975	0.4691	1041	0.1141
712	1.5677	778	1.1566	844	0.7827	910	0.8968	976	0.4597	1042	0.1120
713	1.5481	779	1.1298	845	0.7833	911	0.8964	977	0.4504		
714	1.5285	780	1.1050	846	0.7839	912	0.8957	978	0.4413		
715	1.5093	781	1.0803	847	0.7845	913	0.8951	979	0.4323		

APPENDIX 1—Continued

HbO₂

650 0.3869	716 0.3724	782 0.7485	848 1.1494	914 1.3562	980 1.2513
651 0.3793	717 0.3765	783 0.7549	849 1.1547	915 1.3570	981 1.2470
652 0.3722	718 0.3807	784 0.7613	850 1.1596	916 1.3578	982 1.2430
653 0.3659	719 0.3854	785 0.7681	851 1.1645	917 1.3582	983 1.2393
654 0.3601	720 0.3899	786 0.7743	852 1.1694	918 1.3587	984 1.2351
655 0.3545	721 0.3943	787 0.7808	853 1.1742	919 1.3585	985 1.2305
656 0.3495	722 0.3988	788 0.7874	854 1.1790	920 1.3590	986 1.2260
657 0.3451	723 0.4035	789 0.7941	855 1.1842	921 1.3598	987 1.2219
658 0.3410	724 0.4083	790 0.8005	856 1.1885	922 1.3602	988 1.2173
659 0.3376	725 0.4133	791 0.8070	857 1.1934	923 1.3602	989 1.2133
660 0.3346	726 0.4181	792 0.8134	858 1.1980	924 1.3602	990 1.2087
661 0.3318	727 0.4230	793 0.8197	859 1.2026	925 1.3602	991 1.2043
662 0.3294	728 0.4281	794 0.8264	860 1.2071	926 1.3604	992 1.1992
663 0.3276	729 0.4332	795 0.8330	861 1.2114	927 1.3603	993 1.1939
664 0.3260	730 0.4383	796 0.8392	862 1.2156	928 1.3599	994 1.1893
665 0.3245	731 0.4435	797 0.8458	863 1.2200	929 1.3600	995 1.1848
666 0.3234	732 0.4488	798 0.8524	864 1.2245	930 1.3595	996 1.1789
667 0.3227	733 0.4540	799 0.8588	865 1.2286	931 1.3593	997 1.1733
668 0.3220	734 0.4593	800 0.8653	866 1.2325	932 1.3590	998 1.1694
669 0.3216	735 0.4646	801 0.8716	867 1.2367	933 1.3584	999 1.1637
670 0.3213	736 0.4700	802 0.8780	868 1.2407	934 1.3577	1000 1.1576
671 0.3212	737 0.4754	803 0.8845	869 1.2449	935 1.3569	1001 1.1529
672 0.3212	738 0.4811	804 0.8909	870 1.2490	936 1.3557	1002 1.1476
673 0.3214	739 0.4865	805 0.8973	871 1.2529	937 1.3549	1003 1.1418
674 0.3214	740 0.4920	806 0.9038	872 1.2565	938 1.3545	1004 1.1361
675 0.3211	741 0.4976	807 0.9102	873 1.2601	939 1.3533	1005 1.1302
676 0.3208	742 0.5032	808 0.9164	874 1.2641	940 1.3520	1006 1.1253
677 0.3206	743 0.5089	809 0.9227	875 1.2678	941 1.3511	1007 1.1201
678 0.3205	744 0.5147	810 0.9291	876 1.2710	942 1.3502	1008 1.1136
679 0.3201	745 0.5203	811 0.9354	877 1.2746	943 1.3487	1009 1.1078
680 0.3194	746 0.5259	812 0.9416	878 1.2781	944 1.3468	1010 1.1008
681 0.3186	747 0.5317	813 0.9478	879 1.2814	945 1.3453	1011 1.0949
682 0.3181	748 0.5376	814 0.9539	880 1.2846	946 1.3445	1012 1.0890
683 0.3173	749 0.5436	815 0.9603	881 1.2878	947 1.3428	1013 1.0823
684 0.3163	750 0.5495	816 0.9666	882 1.2907	948 1.3410	1014 1.0758
685 0.3157	751 0.5554	817 0.9728	883 1.2938	949 1.3394	1015 1.0704
686 0.3151	752 0.5613	818 0.9789	884 1.2971	950 1.3374	1016 1.0650
687 0.3140	753 0.5672	819 0.9848	885 1.3000	951 1.3354	1017 1.0580
688 0.3135	754 0.5731	820 0.9911	886 1.3027	952 1.3332	1018 1.0502
689 0.3126	755 0.5791	821 0.9973	887 1.3058	953 1.3313	1019 1.0450
690 0.3123	756 0.5856	822 1.0032	888 1.3084	954 1.3293	1020 1.0378
691 0.3122	757 0.5912	823 1.0091	889 1.3108	955 1.3263	1021 1.0309
692 0.3122	758 0.5974	824 1.0153	890 1.3137	956 1.3240	1022 1.0242
693 0.3123	759 0.6031	825 1.0211	891 1.3165	957 1.3217	1023 1.0172
694 0.3125	760 0.6096	826 1.0273	892 1.3189	958 1.3199	1024 1.0099
695 0.3130	761 0.6157	827 1.0333	893 1.3210	959 1.3172	1025 1.0030
696 0.3140	762 0.6219	828 1.0393	894 1.3235	960 1.3144	1026 0.9973
697 0.3148	763 0.6283	829 1.0449	895 1.3262	961 1.3123	1027 0.9891
698 0.3164	764 0.6345	830 1.0507	896 1.3283	962 1.3099	1028 0.9837
699 0.3181	765 0.6407	831 1.0564	897 1.3304	963 1.3070	1029 0.9739
700 0.3199	766 0.6469	832 1.0621	898 1.3323	964 1.3042	1030 0.9664
701 0.3219	767 0.6535	833 1.0680	899 1.3341	965 1.3018	1031 0.9600
702 0.3243	768 0.6596	834 1.0739	900 1.3365	966 1.2995	1032 0.9517
703 0.3269	769 0.6658	835 1.0797	901 1.3385	967 1.2966	1033 0.9415
704 0.3296	770 0.6720	836 1.0851	902 1.3403	968 1.2928	1034 0.9326
705 0.3323	771 0.6785	837 1.0907	903 1.3420	969 1.2900	1035 0.9267
706 0.3352	772 0.6849	838 1.0962	904 1.3435	970 1.2868	1036 0.9200
707 0.3386	773 0.6911	839 1.1018	905 1.3452	971 1.2838	1037 0.9119
708 0.3418	774 0.6974	840 1.1072	906 1.3467	972 1.2807	1038 0.9045
709 0.3450	775 0.7038	841 1.1128	907 1.3478	973 1.2773	1039 0.8943
710 0.3485	776 0.7101	842 1.1182	908 1.3496	974 1.2735	1040 0.8878
711 0.3524	777 0.7166	843 1.1233	909 1.3507	975 1.2692	1041 0.8783
712 0.3564	778 0.7229	844 1.1286	910 1.3514	976 1.2656	1042 0.8671
713 0.3602	779 0.7297	845 1.1339	911 1.3528	977 1.2624	
714 0.3639	780 0.7360	846 1.1391	912 1.3542	978 1.2590	
715 0.3680	781 0.7422	847 1.1442	913 1.3553	979 1.2549	

ACKNOWLEDGMENTS

The authors thank the Medical Research Council, the Wellcome Trust, and Hamamatsu Photonics KK for generous financial support.

REFERENCES

1. Jöbsis, F. F. (1977) *Science* **198**, 1264-1267.
2. Brazy, J. E., and Lewis, D. V. (1986) *Pediatrics* **108**, 983-987.
3. Ferrari, M., De Marchis, C., Giannini, I., Nicola, A., Agostino, R., Nodari, S., and Bucci, G. (1986) *Adv. Exp. Med. Biol.* **200**, 203-212.
4. Wyatt, J. S., Cope, M., Delpy, D. T., Edwards, A. D., Wray, S. C., and Reynolds, E. O. R. (1986) *Lancet* **2**, 1063-1066.
5. Edwards, A. D., Wyatt, J. S., Richardson, C., Delpy, D. T., Cope, M., and Reynolds, E. O. R. (1988) *Lancet* **2**, 770-771.
6. Elwell, C. E., Cope, M., Edwards, A. D., Wyatt, J. S., Reynolds, E. O. R., and Delpy, D. T. (1992) *Adv. Exp. Med. Biol.* **317**, 235-245.
7. Hoshi, Y., and Tamura, M. (1993) *J. Appl. Physiol.* **75**(4), 1842-1846.
8. Hampson, N. B., and Piantadosi, C. A. (1988) *J. Appl. Physiol.* **64**, 2449-2457.
9. Cheatle, T. R., Potter, L. A., Cope, M., Delpy, D. T., and Coleridge Smith, P. D. (1991) *Br. J. Surg.* **78**, 405-408.
10. De Blasi, R. A., Cope, M., Elwell, C. E., Safoue, F., and Ferrari, M. (1993) *Eur. J. Appl. Physiol.* **67**, 20-25.
11. Cope, M., van der Zee, P., Essenpreis, M., Arridge, S. R., and Delpy, D. T. (1991) *Proc. SPIE-Int. Soc. Opt. Eng.* **1431**, 251-262.
12. Cope, M. (1991) Ph.D. thesis, University College London.
13. Cope, M., Delpy, D. T., Wray, S., Wyatt, J. S., and Reynolds, E. O. R. (1989) *Adv. Exp. Med. Biol.* **247**, 33-40.
14. Cady, E. B., Wyatt, J. S., Takei, Y., Lorek, A., Cooper, C. E., Edwards, A. D., Roth, S. C., Peebles, D. M., Aldridge, R. F., Wylezinska, M., Delpy, D. T., and Reynolds, E. O. R. (1993) *Proc. 12th SMRM New York*, August 14-20, 1502.
15. Delpy, D. T., Gordon, R. E., Hope, P. L., Parker, D., Reynolds, E. O. R., Shaw, D., and Whitehead, M. D. (1982) *Paediatrics* **70**, 310-313.
16. Lorek, A., Takei, Y., Cady, E. B., Wyatt, J. S., Penrice, J., Edwards, A. D., Peebles, D., Wylezinska, M., Owen-Reece, H., Kirkbride, V., Cooper, C. E., Aldridge, R. F., Roth, S. C., Brown, G., Delpy, D. T., and Reynolds, E. O. R. (1994) *Pediatr. Res.* **36**, 699-706.
17. Delpy, D. T., Cope, M., van der Zee, P., Arridge, S. R., Wray, S., and Wyatt, J. S. (1988) *Phys. Med. Biol.* **33**(12), 1433-1442.
18. van der Zee, P., Cope, M., Arridge, S. R., Essenpreis, M., Potter, L. A., Edwards, A. D., Wyatt, J. S., McCormick, D. C., Roth, S. C., Reynolds, E. O. R., and Delpy, D. T. (1992) *Adv. Exp. Med. Biol.* **316**, 143-153.
19. Essenpreis, M., Elwell, C. E., van der Zee, P., Arridge, S. R., and Delpy, D. T. (1993) *Appl. Opt.* **32**(4), 418-425.
20. Cope, M., and Delpy, D. T. (1988) *Med. Biol. Eng. Comp.* **26**(3), 289-294.
21. Hazeki, O., and Tamura, M. (1989) *Adv. Exp. Med. Biol.* **248**, 63-69.
22. Hazeki, O., Seiyama, A., and Tamura, M. (1987) *Adv. Exp. Med. Biol.* **215**, 283-289.
23. Piantadosi, C. A. (1993) *Methods Toxicol.* **2**, 107-126.
24. Wickramasinghe, Y., Thorniley, M., Rolfe, P., Houston, R., Livera, L. N., and Faris, F. (1990) *Proc. 12th Ann. Int. Conf. IEEE Eng. Biol. Soc.*, 1545-1554.
25. Crowe, J. (1986) Ph.D. thesis, Oxford University.
26. Wickramasinghe, Y., and Rolfe, P. (1993) *EC Biomed. Newslett.* **2**, 5.
27. Wilson, D. F., Rumsey, W. L., Green, T. J., and Vanderkooi, J. M. (1988) *J. Biol. Chem.* **263**, 2712-2718.
28. Peterson, L. C., Nicholls, P., and Degn, H. (1976) *Biochim. Biophys. Acta* **452**, 59-65.
29. Piantadosi, C. A., Hemstreet, T. M., and Jöbsis-Vandervliet, F. F. (1986) *Crit. Care Med.* **14**(8), 698-706.
30. Kariman, K., Hempel, F. G., and Jöbsis, F. F. (1983) *J. Appl. Physiol.* **55**(4), 1057-1063.
31. Honig, C. R., Connett, R. J., and Gayeski, T. E. J. (1992) *Med. Sci. Sports Exercise* **24**, 47-53.
32. Arridge, S. R., Cope, M., and Delpy, D. T. (1992) *Phys. Med. Biol.* **37**, 1531-1560.
33. Arridge, S. R., Schweiger, M., Hiraoka, M., and Delpy, D. T. (1993) *Med. Phys.* **20**(2), 299-309.
34. van der Zee, P., Essenpreis, M., and Delpy, D. T. (1993) *Proc. SPIE-Int. Soc. Opt. Eng.* **1888**, 454-465.
35. van der Zee, P. (1993) Ph.D. thesis, University of London.
36. van Kuilenburg, A. B. P., Dekker, H. L., van den Bogert, C., Nieboer, P., van Gelder, B. F., and Muijsers, A. O. (1991) *Eur. J. Biochem.* **199**, 615-622.
37. Madsen, S. J., Wilson, B. C., Patterson, M. S., Park, D. P., Jacques, S. L., and Hefetz, Y. (1992) *Appl. Opt.* **31**, 3509-3517.
38. Wray, S., Cope, M., Delpy, D. T., Wyatt, J. S., and Reynolds, E. O. R. (1988) *Biochim. Biophys. Acta* **933**, 184-192.
39. Cooper, C. E., Matcher, S. J., Wyatt, J. S., Cope, M., Brown, G. C., Nemoto, E. M., and Delpy, D. T. (1994) *Biochem. Soc. Trans.* **22**, 974-980.